International Journal of Heat and Mass Transfer 112 (2017) 918–925

Contents lists available at ScienceDirect

International Journal of Heat and Mass Transfer

journal homepage: www.elsevier.com/locate/ijhmt

Thermocapillary effect on the absolute and convective instabilities of film flows down a fibre

Rong Liu [a], Zijing Ding [b,*], Zhiqiang Zhu [c]

[a] School of Mechanical and Electrical Engineering, Gui Lin University of Electronic Technology, Gui Lin 541004, China
[b] School of Mathematics, University of Bristol, Bristol BS8 1TW, United Kingdom
[c] National Microgravity Laboratory, Institute of Mechanics, Chinese Academy of Sciences, Beijing 100190, China

ARTICLE INFO

Article history:
Received 25 February 2017
Received in revised form 8 May 2017
Accepted 8 May 2017
Available online 19 May 2017

Keywords:
Film flow
Marangoni effect
Absolute and convective instabilities

ABSTRACT

We consider the motion of a gravity-driven flow down a uniformly heated vertical fibre. This flow exhibits rich dynamics including the formation of droplets, or beads, driven by a Rayleigh-Plateau mechanism modified by the presence of gravity as well as the thermocapillarity at the interface. A spatio-temporal stability analysis is performed to investigate the effect of thermocapillarity (Marangoni effect) on the convective/absolute instability (CI/AI) characteristics of the problem. We also performed a numerical simulation of Eq. (30) on the nonlinear evolution of the film to connect the breakup behaviours with the CI/AI characteristics. Our numerical results showed that for various Marangoni number (*Ma*), breakup of the film mainly occurs in the AI regime. With the increase of *Ma*, the film has a tendency to break up into droplets due to the enhancement of the absolute instability.

1. Introduction

The dynamics of a liquid film flowing down a vertical fibre has been encountered in many industrial applications, for example, draining, coating of insulation on a wire, and the protection coating tube walls [1]. It is well known that a cylindrical thread or jet has a tendency to break up into spherical droplets to reduce the surface area due to a surface tension driven mechanism (the Rayleigh-Plateau instability) [2]. For a film flowing down a slender cylindrical fibre, the Rayleigh-Plateau mechanism is modified by the flow driven by gravity. At small Reynolds numbers, the film is always unstable and spontaneously breaks up into a wave train consisting of axisymmetric droplets.

Experimental investigation on the gravity-driven flow on a fibre was performed first by Quéré [3]. The results showed that two different kinds of behaviour can be observed according to the film thickness: For a thick film on a slender fibre, drops develop due to the Rayleigh instability and flow downwards. Some of drops grow by swallowing the other ones, and quickly fall, leaving behind them a thick film which breaks up in turn into droplets. For a thin film on a large fibre, the breakup process may be arrested by the mean flow. The arrest by the mean flow of the latter case was investigated by many authors [4–6] using a lubrication-type (Benney-like) equation for the film thickness wherein the fibre radius a is much larger than the film thickness h.

Kliakhandler et al. [7] studied experimentally the case where the film thickness is larger than the fibre radius. Three qualitatively different regimes of the interfacial patterns in the form of beads were observed in the experiments. In their experiments, the film is at least twice as thick as the fibre radius. Therefore, the previously derived Benney-like equations under the assumption of $h \ll a$ do not apply there. The authors proposed an evolution equation which does not rely on the previously made lubrication-type assumptions. Two typical regimes at relatively small flow rate are well predicted by their model. However, this equation fails to capture a regime that features beads separated by relatively long flat thin-film regions. Craster and Matar [8] derived a new evolution equation similar to that used by Kliakhandler et al. [7] and revisited the same problem. The authors showed that numerical solutions of their model equation yield good agreement with the experimental observations reported by Kliakhandler et al. [7].

All modelling mentioned above are valid for the Reynolds number $Re \sim \mathcal{O}(1)$ or smaller due to the assumption of negligible inertia effects. Ruyer-Quil et al. [9] formulated a two-equation model for the film thickness h and flow rate q using a weighted residuals approach. This model accounting for inertia and streamwise viscous diffusion is valid for both small and $\mathcal{O}(1)$ aspect ratios of h/a. Comparisons between the numerical result and experimental results show good agreement in both linear and nonlinear regimes.

* Corresponding author.
E-mail addresses: rongliu@guet.edu.cn (R. Liu), z.ding@bristol.ac.uk (Z. Ding), zhuzhiqiang@imech.ac.cn (Z. Zhu).

http://dx.doi.org/10.1016/j.ijheatmasstransfer.2017.05.030
0017-9310/

In practical processes, a more complex situation is that the fibre-coating is operated in a cooling environment. In glass manufacturing process, glass fibres are made by drawing molten glass through an array of small diameter bushings. In order to enhance the heat removal from the fibres, they are sprayed with water from atomizing nozzles [10]. In this situation where the coating film is cooled by the environment, the Rayleigh-Plateau instability is modified by thermocapillary stress due to surface tension variations produced by temperature disturbances at the interface.

The effect of thermocapillarity on the dynamics of thin films on cylinders have given rise to broad scientific interest for its technological importance. Dávalos-Orozco and You [11] performed a linear stability analysis on the Navier-Stokes equations to investigate the three-dimensional thermocapillary instability of a fluid film coating the outside or the inside of a cylinder in the absence and in the presence of gravity. The results showed that pure thermocapillarity is possible to excite non-axisymmetric unstable mode. Liu and Liu [12] studied the longwave stability of thin film flowing down a uniformly heated vertical fibre. The results showed that the Marangoni instability and the Rayleigh-Plateau instability reinforce each other. With the increase of the thermocapillary effect, the coating flow has a tendency to break up into smaller droplets. Ding and Wong showed that these smaller droplets could also be unstable due to the azimuthal disturbances and would evolve into an asymmetric state [13]. Recently, Moctezuma-Sánchez, and Dávalos-Orozco [14] studied the non-axisymmetric longwave instability of a thin viscoelastic liquid film flowing down a vertical heated cylinder. The results show that, in comparison with the Newtonian case, it is easier to excite the azimuthal modes when viscoelasticity and thermocapillarity destabilize at the same time.

In experiments, the instability characteristics can be categorized by the location where instability growth can be visually detected. The concept of the convective/absolute stability was first developed in the context of plasma physics [15,16] and later has been extended to the problems of hydrodynamics [17]. Transitions between different wave regimes in coating flows on a fibre can be understood within the framework of absolute and convective instabilities. Convectively unstable flows behave as spatial amplifiers of the incoming perturbations: at a fixed point in the laboratory frame of reference, the signal eventually dies out. Whereas, absolutely unstable flows display intrinsic self-sustained dynamics: although advected, the perturbation is so strongly amplified that it contaminates the entire flow region (downstream and upstream).

Joo and Davis [18] have studied the absolute and convective stabilities for viscous falling films on a vertical plate. Recently, the absolute and convective instabilities of flows with a cylindrical free surface give rise to broad scientific interest. Duprat et al. [19] have studied the absolute and convective stabilities for a viscous film flowing down a vertical fibre. The authors have reported a flow regime diagram which identifies, depending on the fibre radius and the flow rate, the AI/CI characteristics. At large or small film thicknesses, the instability is convective, whereas absolute instability is observed in an intermediate range of film thicknesses for fibres of small enough radius. Balestra et al. [20] studied the linear spatio-temporal stability of heated coaxial jet flows. The results showed that the temperature ratio and the velocity ratio between the core jet play important roles in the transition from convectively to absolutely unstable flows.

In the present paper, we are interested in the aspect of the absolute and convective instabilities of a film flowing down a vertical fibre with a temperature difference between the fibre wall and the film interface.

This paper is organized as follows. In Section 2 the mathematical formulation of the physical model is presented. In Section 3 we present the results and discussions. In Section 4 we summarize the results and present the conclusions.

2. Mathematical formulation

As shown in Fig. 1, a Newtonian fluid, of constant viscosity μ and density ρ, flows down a vertical fibre of radius $r = a$ under gravity g. The initial radius of the fluid ring measured from the centre of the fibre is $r = R$. The temperatures of the fibre wall and the interface of the film are T_a and T_i.

The dynamics of the axisymmetric flow of the film is governed by the Navier-Stokes equations,

$$u_r + \frac{u}{r} + w_z = 0, \tag{1}$$

$$u_t + uu_r + wu_z = -\frac{p_r}{\rho} + \frac{\mu}{\rho}\left[u_{rr} + \frac{u_r}{r} - \frac{u}{r^2} + u_{zz}\right], \tag{2}$$

$$w_t + uw_r + ww_z = g - \frac{p_z}{\rho} + \frac{\mu}{\rho}\left[w_{rr} + \frac{w_r}{r} + w_{zz}\right], \tag{3}$$

$$T_t + uT_r + wT_z = \kappa\left[T_{rr} + \frac{T_r}{r} + T_{zz}\right], \tag{4}$$

where t denotes time, u and w denote the radial (r) and axial (z) velocity components, p denotes the pressure, T denotes the temperature, κ denotes the thermal diffusivity. Note that unless stated otherwise, the subscript denotes partial differentiation.

At the fibre surface ($r = a$), no penetration and no slip conditions for the velocities are

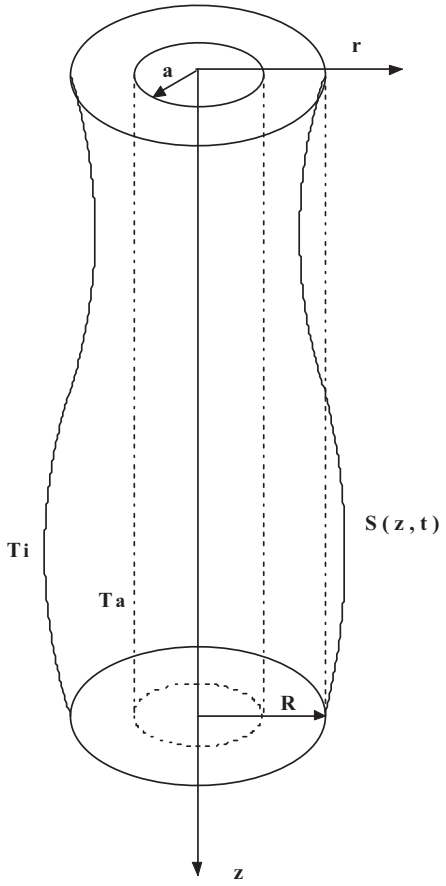

Fig. 1. Sketch of the geometry of a film flow coating a fibre.

$$u = w = 0. \tag{5}$$

The temperature at the fibre wall is prescribed,

$$T = T_a. \tag{6}$$

At the free surface $r = S(z,t)$, the shear stress is balanced by the thermocapillary force,

$$\boldsymbol{t}\cdot\boldsymbol{T}\cdot\boldsymbol{n} = \boldsymbol{t}\cdot\nabla_s\sigma, \tag{7}$$

and the normal stress is balanced by surface tension times the curvature,

$$\boldsymbol{n}\cdot\boldsymbol{T}\cdot\boldsymbol{n} = 2\sigma H, \tag{8}$$

here $\boldsymbol{T}$ is the stress tensor, $\boldsymbol{n}$ and $\boldsymbol{t}$ are the unit vectors normal and tangent to the interface expressed as

$$\boldsymbol{t} = \frac{(1, S_z)}{\sqrt{1+S_z^2}}, \tag{9}$$

$$\boldsymbol{n} = \frac{(-S_z, 1)}{\sqrt{1+S_z^2}}, \tag{10}$$

and $2H$ is the surface principal curvature. The surface tension is assumed to be linearly dependent on the temperature,

$$\sigma = \sigma_0 - \gamma(T_i - T_0), \tag{11}$$

where γ is a constant coefficient and T_0 is the temperature of the reference state.

The kinematic boundary condition on the free surface is

$$S_t + \frac{1}{S}\frac{\partial}{\partial z}\int_a^S wr\,\mathrm{d}r = 0. \tag{12}$$

The balance between heat supply to and heat loss from the surface is given by Newton's law of cooling,

$$-\chi\boldsymbol{n}\cdot\nabla T = q(T - T_\infty), \tag{13}$$

in which χ is the thermal conductivity of the liquid and q is the heat transfer coefficient describing the rate of heat transport from the liquid to the ambient gas with temperature T_∞ far away from the interface.

2.1. Scaling and asymptotic reduction

We assume that the radius of the fluid ring, R, is much smaller than the wavelength L. The dimensionless variables denoted by stars are defined as

$$r = Rr^*, z = Lz^*, p = \rho gLp^*, t = LV^{-1}t^*, w = Vw^*,$$
$$u = \epsilon Vu^*, T - T_\infty = \Delta TT^*, \tag{14}$$

where $V \equiv \rho gR^2/\mu$. The length scale L is taken to be the capillary length $L = \sigma/\rho gR$. The Bond number $Bo = \rho gR^2/\sigma$ naturally appears and in the experiments it is typically small. The parameter $\epsilon = R/L = Bo$ is for a low Bond number and surface-tension-dominated theory.

The dimensionless Navier-Stokes equations become

$$u_r + \frac{u}{r} + w_z = 0, \tag{15}$$

$$\epsilon^4 Re(u_t + uu_r + wu_z) = -p_r + \epsilon^2\left[u_{rr} + \frac{u_r}{r} - \frac{u}{r^2} + \epsilon^2\frac{\partial^2 u}{\partial z^2}\right], \tag{16}$$

$$\epsilon^2 Re(w_t + uw_r + ww_z) = 1 - p_z + \left[w_{rr} + \frac{w_r}{r} + \epsilon^2 w_{zz}\right]. \tag{17}$$

$$\epsilon Re(T_t + uT_r + wT_z) = \frac{1}{Pr}\left[T_{rr} + \frac{T_r}{r} + \epsilon^2 T_{zz}\right], \tag{18}$$

where the Prandtl number is defined as $Pr = \nu/\kappa$, and the Reynolds number is defined as $Re = \rho VL/\mu$. Note that the Reynolds number can be expressed as $Re = \sigma\rho R/\mu^2$. This parameter is independent of g. This means that the present problem is for surface tension dominant flow which is mainly driven by surface tension instead of gravity.

For simplicity we have dropped the star for all the dimensionless variables. Assuming $\epsilon \ll 1$ and $Re \sim \mathcal{O}(1)$, we can remove the contributions of the inertial terms. We now seek solutions as regular perturbation expansions in

$$\begin{cases} u = \epsilon u_0 + \epsilon^2 u_1 + \ldots, \\ w = w_0 + \epsilon w_1 + \ldots, \\ p = p_0 + \epsilon p_1 + \ldots, \\ T = T_0 + \epsilon T_1 + \ldots, \end{cases} \tag{19}$$

and the leading-order Navier-Stokes equations are given by

$$w_{0rr} + \frac{w_{0r}}{r} = p_{0z} - 1, \tag{20}$$

$$T_{0rr} + \frac{T_{0r}}{r} = 0. \tag{21}$$

The leading-order normal and tangential stress balances at the surface are

$$p_0 = \frac{1}{S} - \epsilon^2 S_{zz}, \quad w_{0r} = -\epsilon Ma(S_z T_{ir} + T_{iz}), \tag{22}$$

where the Marangoni number is defined as $Ma = \gamma\Delta T/\mu V$.

The temperature at $r = a$ is

$$T_0 = 1, \tag{23}$$

and Newton's law of cooling at the surface $r = S$ is

$$T_{0r} + BiT_0 = 0, \tag{24}$$

where the Biot number is defined as $Bi = qR/\chi$. We obtain the distribution of the temperature as

$$T_0 = \frac{Bi\ln\frac{r}{S} - \frac{1}{S}}{Bi\ln\frac{a}{S} - \frac{1}{S}}. \tag{25}$$

At the interface, the temperature is

$$T_i(z) = \frac{-1}{BiS\ln\frac{a}{S} - 1}. \tag{26}$$

The velocity $w_0(r,z,t)$ is

$$w_0 = (1 - p_{0z})\left[\frac{1}{4}(a^2 - r^2) + \frac{1}{2}S^2\ln\frac{r}{a}\right] - \epsilon MaT_{iz}S\ln\frac{r}{a}. \tag{27}$$

Substituting w into the continuity equation, we obtain the expression of u,

$$u_0 = -\frac{1}{r}\left\{\frac{1}{16}p_{0zz}(a^2 - r^2) + \left[\frac{S^2}{2}(1 - p_{0z}) - \epsilon MaT_{iz}S\right]_z\left[\frac{1}{2}r^2\ln\left(\frac{r}{a}\right) - \frac{1}{4}(r^2 - a^2)\right]\right\}. \tag{28}$$

We can define a stream function $\Psi(r) = \int_a^r ru\,\mathrm{d}r$, and obtain $\Psi(r)$ as

$$\Psi = (1 - p_{0z})\left[-\frac{1}{16}(r^4 - a^4) + \frac{1}{4}S^2r^2\ln\left(\frac{r}{a}\right) - \frac{1}{8}(S^2 - a^2)(r^2 - a^2)\right] - \epsilon MaT_{iz}S\left[\frac{r^2}{2}\ln\frac{r}{a} - \frac{1}{4}(r^2 - a^2)\right], \tag{29}$$

and the flow rate, $Q = \Psi(S)$, along the fibre can be expressed as

$$Q(S) = (1 - p_{0z})\left[\frac{1}{4}S^4 \log\frac{S}{a} + \frac{(3S^2 - a^2)(a^2 - S^2)}{16}\right] - \epsilon Ma T_{iz}\left[\frac{S^3}{2}\ln\frac{S}{a} - \frac{S}{4}(S^2 - a^2)\right], \tag{30}$$

where

$$T_{iz} = \frac{BiS_z(\ln\frac{a}{S} - 1)}{(BiS\ln\frac{a}{S} - 1)^2}. \tag{31}$$

Substituting Q into the kinematic boundary condition yields an evolution equation for $S(z,t)$ as

$$\partial_t S^2 + 2\partial_z Q(S) = 0. \tag{32}$$

For unperturbed state, the dimensionless flow rate

$$\bar{Q} = -\frac{1}{4}\log a + \frac{(3 - a^2)(a^2 - 1)}{16}, \tag{33}$$

is the function of a. In experiments, one needs to know the mass flux q^* which can be expressed as

$$q^* = 2\pi(\rho V R^2)\bar{Q} = \epsilon Re \cdot (\mu R)\bar{Q}(a). \tag{34}$$

Thus, the mass flux rate q^* can be converted from the flow rate $\bar{Q}$.

3. Results and discussions

3.1. Absolute and convective instabilities

Let us now consider the linear stability of the problem. A small periodic disturbance in the streamwise direction is imposed on the film such that the film thickness can be decomposed into a basic state component $\bar{S}$, and a small disturbance with amplitude $\hat{S}$,

$$S = \bar{S} + \hat{S}e^{i(kz - \omega t)}, \tag{35}$$

in which $\bar{S} = 1$, ω is the frequency and k is the wavenumber.

Substituting Eq. (35) into Eq. (32) yields a dispersion relation

$$\mathcal{D}(k,\omega) = -i\omega + \left\{\frac{1}{16}k^2(k^2\epsilon^2 - 1)(4\ln\frac{1}{a} - a^4 + 4a^2 - 3) + \frac{ik}{2}(a^2 - 1 - 2\ln a)\right\} + \frac{\epsilon}{4}k^2 MaBi\frac{(a^2 - 1 - 2\ln a)(\ln a - 1)}{(Bi\ln a - 1)^2} = 0. \tag{36}$$

The maximum real growth rate

$$\max\omega_i = \frac{A}{64\epsilon^2}\left(1 + 4\epsilon Ma\frac{B}{A}\right)^2 \tag{37}$$

is realized at the wavenumber

$$k_m = \frac{1}{\sqrt{2}\epsilon}\left(1 + 4\epsilon Ma\frac{B}{A}\right)^{1/2}, \tag{38}$$

in which the coefficients A and B are

$$A = 4\ln\frac{1}{a} - a^4 + 4a^2 - 3,$$
$$B = -Bi\frac{(a^2 - 1 - 2\ln a)(\ln a - 1)}{(Bi\ln a - 1)^2}. \tag{39}$$

The cut-off wavenumber at which the real growth rate is zero is

$$k_c = \frac{1}{\epsilon}\left(1 + 4\epsilon Ma\frac{B}{A}\right)^{1/2}. \tag{40}$$

It can be shown that the sign of B/A is positive. So, with the increase of the Marangoni number, both the wavenumber of the most unstable mode and the cut-off wavenumber increase.

In spatio-temporal stability analysis, both the wavenumber k and the frequency ω are complex numbers. The solution of the impulsive response can be expressed in the form of

$$G(z,t) = \frac{1}{2\pi}\int_A\int_F \frac{e^{i(kz - \omega t)}}{\mathcal{D}(k,\omega)}\mathrm{d}\omega\mathrm{d}k, \tag{41}$$

where the Bromwich contour F in the ω-plane is a horizontal line lying above all the singularities to satisfy causality, and the integration path A lies inside the analyticity band around the k-axis. The absolute/convective instability is determined by the long-time behaviour of the impulse response $G(z,t)$ along the rays $z/t = \text{const}$. The spatio-temporal asymptotic behaviour of a perturbation is determined by the complex solutions $k = k(V_s)$ (saddle points) of the equation $\partial\omega/\partial k = V_s = z/t$ along a given ray $V_s = \text{const}$. At a fixed location z, the long-time behaviour is determined by the study of the behaviour of the disturbance with a zero group velocity, i.e.

$$\left.\frac{\partial\omega}{\partial k}\right|_{k=k_0} = 0, \tag{42}$$

where $\omega_0 = \omega(k_0)$ is called the absolute frequency and k_0 the saddle point. If $\mathrm{Im}(\omega_0) > 0/\mathrm{Im}(\omega_0) < 0$ the instability is said to be absolutely/convectively unstable. It should be noted that the saddle point k_0 used to identify absolute/convective instability must satisfy the Briggs-Bers [15,16] collision criterion, i.e. the saddle point must be a pinch point produced by two distinct spatial branches of solutions of the dispersion relation coming from the upper and lower half-k-planes. The method to study absolute/convective instability (AI/CI) is a standard procedure. For more detail on AI/CI problems, we refer the reader to a good review article by Huerre and Monkewitz [17].

In Eq. (32), the parameters Ma and Bi play roles in the dispersion relation. As $Ma = 0$ or $Bi = 0$, the thermocapillarity is absent and the dispersion relation is reduced to the isothermal case. Liu and Liu [12] have performed a temporal linear stability analysis on the effect of thermocapillarity on the coating flow on a vertical fibre. In this subsection, we will perform a spatio-temporal analysis to study the effects of thermocapillarity on the AI/CI characteristics.

In order to investigate the influence of the Marangoni effect on the AI/CI characteristics, we compute ω_0 for various parameters of a, Bo, Bi and Ma. In Fig. 2, the locus of ω_0 with the increase of Ma are plotted for various a at $Bi = 1$ and $Bo = 0.4$. As shown in this figure, at $Ma = 0$ the negative imaginary part of ω marked by a circle corresponds to convective instability. In each curve of the locus, the imaginary part of ω_0 increases with Ma. As Ma exceeds a certain value, $\mathrm{Im}(\omega_0)$ becomes positive. This means that the increase of Marangoni effect enforces the absolute instability.

In order to know the influence of Ma on the AI/CI characteristics for different flow regimes, we present in Figs. 3 and 4 the AI/CI boundaries for various Ma and Bi in the $a - Bo$ plane. The range of parameter a is $(0,1)$. The model is valid for small ϵ, thus when presenting the results the range of Bo is confined in $(0, 0.5)$.

In Fig. 3(a) for small Biot number of $Bi = 0.1$, with the increase of Ma the AI/CI boundaries extend towards the larger Bo regions. As $a \to 0, Bo$ at the boundary curves increases as Ma increases from 0 to 1. The AI/CI boundaries for a larger Biot number of $Bi = 1$ are plotted in Fig. 3(b) for various Marangoni numbers. As Ma increases to 0.2, a new branch of the boundary begins to appear near the region of $a = 1$. As Ma increases further, the two branches of the boundary coalesce and the AI regime extends in the $a - Bo$

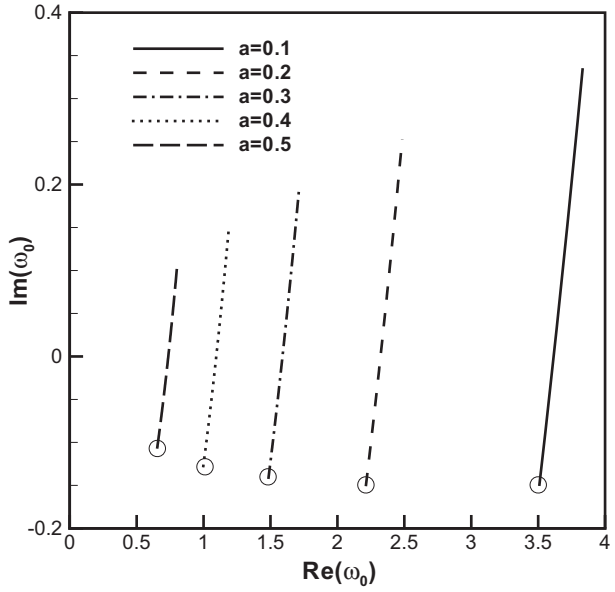

Fig. 2. The locus of the absolute frequency ω_0 as Ma increases from 0 to 1.0 for various $a = 0.1 - 0.5$, $Bo = 0.4$ and $Bi = 1$. The values of ω_0 at $Ma = 0$ are marked by circles.

plane. As shown in Fig. 3(c) and (d) for larger Biot numbers of $Bi = 10$ and 100, the AI regime always extends in the $a - Bo$ plane with the increase of Ma. This means that with the increase of the Marangoni effect promotes the absolute instability for a film interface with a non-zero Biot number.

In order to know the effect of Biot number on the AI/CI characteristics of the problem, we plot the boundaries of the AI/CI regime in Fig. 4. For $Bi \to 0$ and ∞, no Marangoni effect exists. For small Biot numbers, with the increase of Bi the AI regime extends in the $a - Bo$ plane. For large Biot numbers, the boundary shrinks towards that with no Marangoni effect.

3.2. Breakup behaviour and transient solutions

In this subsection, we will study the Marangoni effect on the nonlinear evolution of the film. The computational domain is set to be the interval $[-l/2, l/2]$, and periodical condition is imposed to simulate the evolution. The solution of the position of the interface is approximated by a Fourier series:

$$S(z,t) = \sum_{n=-N/2}^{N/2} \hat{s}_n(t) \exp(i2\pi nz/l), \tag{43}$$

where $\hat{s}_n$ is the Fourier coefficient and N is the number of Fourier modes. A Fourier pseudospectral method is used to provide the discretization in space. The second-order Runge-Kutta method for stiff problems was used for the time advance and the relative error is set to be less than 10^{-6}.

When break-up occurs, there is numerical evidence that the model can break down with some form of finite-time blow-up. Near the blow-up time, the interface deformation with largest amplitude undergoes rapid growth to the point of becoming comparable to the fibre radius, i.e. $S(z,t) = a$. As $S(z,t) - a$ approaches to zero, some of the coefficients of the long-wave model equation become large, leading to a very stiff problem in which the numerical simulation usually breaks down. It is natural to take

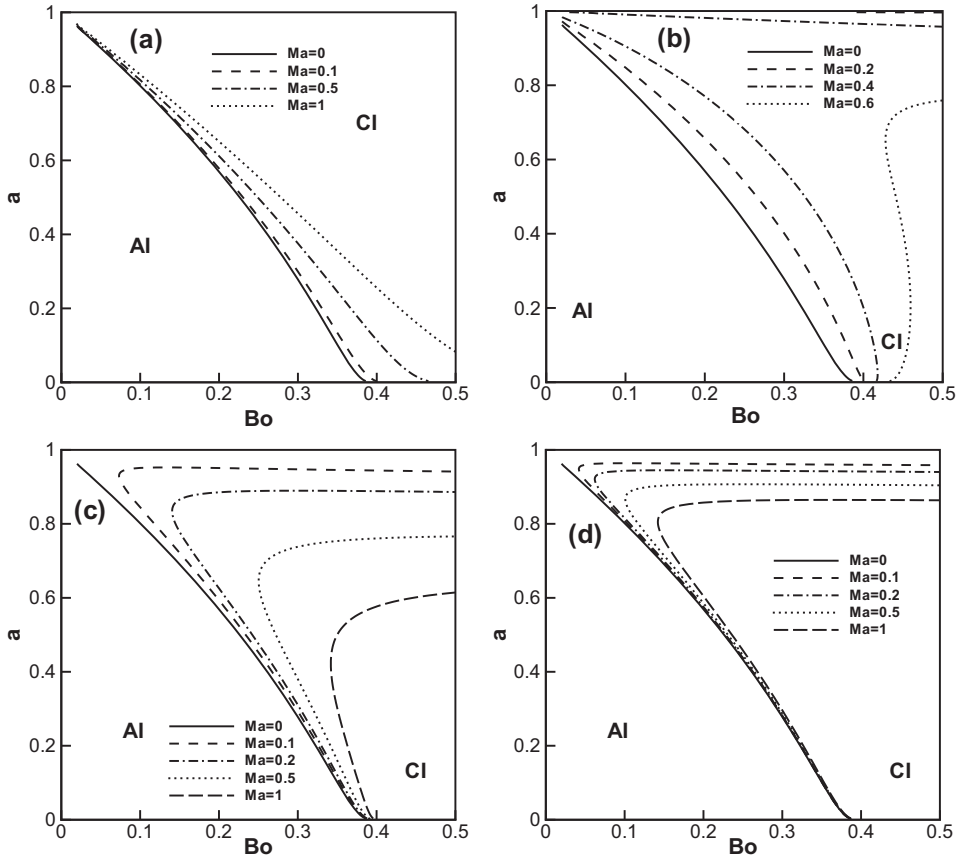

Fig. 3. The boundaries between the convective and absolute instabilities in the $a - Bo$ plane for various Ma. (a) $Bi = 0.1$, (b) $Bi = 1$, (c) $Bi = 10$, (d) $Bi = 100$.

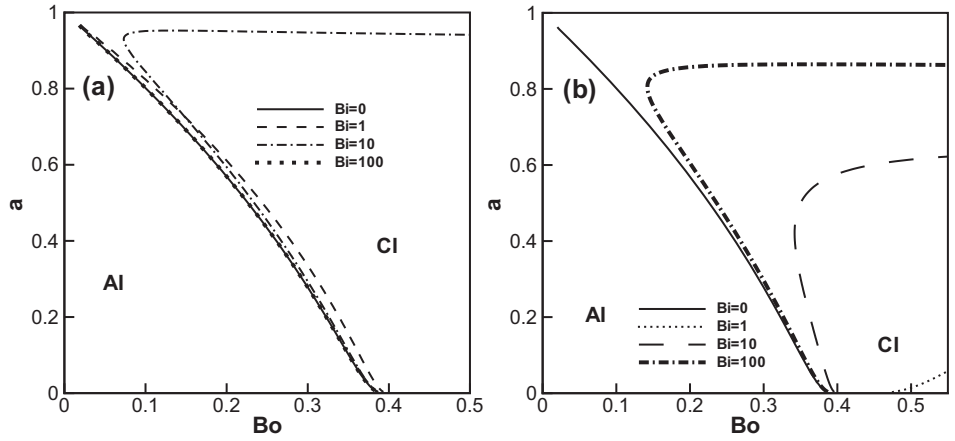

Fig. 4. The boundaries between the convective and absolute instabilities for various *Bi*. (a) $Ma = 0.1$, (b) $Ma = 1.0$.

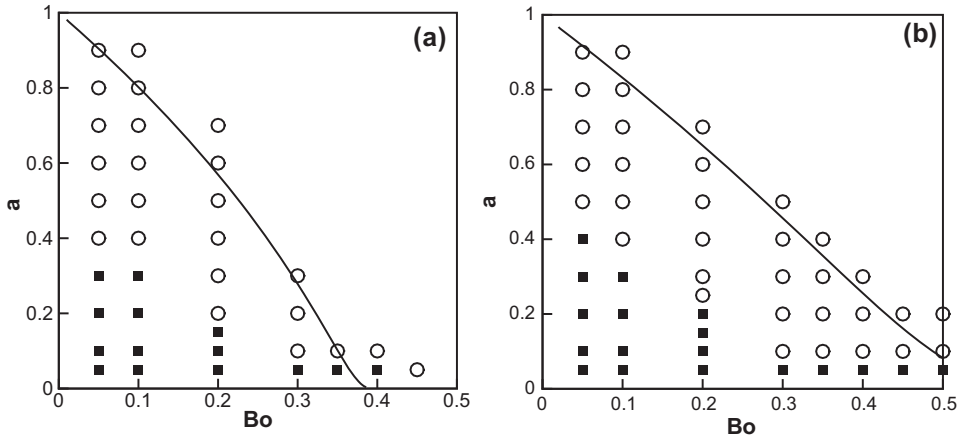

Fig. 5. Parametric space in the $a - Bo$ plane for small Biot number of $Bi = 0.1$. Breakup and no-breakup regimes are marked by squares and circles. (a) $Ma = 0$, (b) $Ma = 1.0$.

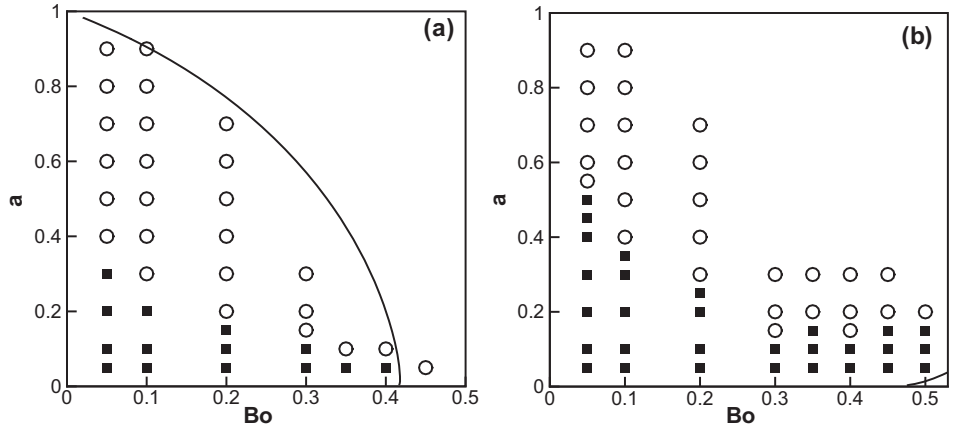

Fig. 6. Parametric space in the $a - Bo$ plane for medium Biot number of $Bi = 100$. Breakup and no breakup regimes are marked by squares and circles. (a) $Ma = 0.4$, (b) $Ma = 1.0$.

the tendency for the interface location S approaches to a, as an indication of the breakup.

We will test the breakup behaviour based on the numerical solution of Eq. (32) for a wide range of parameters of a and Bo. It is a very difficult task to determine whether breakup eventually occurs from the numerical results within a limited time period. In general, the breakup behaviour is a local behaviour which is not sensitive to initial and boundary conditions. Perform numerical simulations on nonlinear evolution in a long spacial domain is very costly numerically. In our computation, we apply a convenient way to examine the breakup. We can test the breakup case in a relatively short spacial domain for a relatively long time period. If

breakup occurs, we then compute it in a long spacial domain. We found that the breakup behaviour is insensitive to the length of spacial domain. For this reason, we can easily observe the breakup in a relatively short domain. In each no-breakup case, when the film reaches a saturated state the interface is in the form of a quasi-steady travelling wave. The snapshots of different time are qualitatively similar. In general, $t = 1000$ is enough for the film to reach quasi-steady state.

In Figs. 5 and 6, the breakup and no-breakup regimes are marked by the shaded squares and hollow circles in the parametric $a - Bo$ plane. The boundaries between convective and absolute instabilities are plotted by solid lines to show the relation between the AI/CI boundary and the breakup behaviours. In Fig. 5, the breakup and non-breakup regimes are presented for small Biot number of $Bi = 0.1$. As shown in Fig. 5(a) and (b), almost all the breakup points are located in the AI regime. At small Bo, the values of a of the AI regime are much lower than the AI/CI boundary. The maximum a of the AI regime gradually decreases with the increase of Bo. As Bo slightly exceeds the CI/AI boundary, the breakup regime disappears. In Fig. 6, the breakup and non-breakup regimes are presented for medium Biot number of $Bi = 100$. In Fig. 6(a) for $Ma = 0.4$ and 1.0, almost all breakup points are confined in the AI regime.

In order to know the properties of the solutions which are naturally selected, we perform numerical simulations on relatively long domains. Starting from a film surface of uniform radius seeded with random disturbances with an amplitude in the range of $0–10^{-3}$ on a spatial domain with a length of l, the profiles of the free surface are plotted in Fig. 7–9 for several typical parameters.

For $a = 0.4$, $Bo = 0.3$, $Bi = 0.1$, the flow is convectively unstable for $Ma = 0$ as shown in Fig. 3(a). As Ma increases to 1.0, the flow becomes absolutely unstable. In Fig. 7, the profiles of the interface for $Ma = 0$ to 2.0 are shown. Even for absolutely unstable case with a high Ma, no breakup phenomenon has been observed in Fig. 7. The interface is in the form of a quasisteady travelling wave for each case. As shown in Eq. (36) that the wavenumber of the most unstable mode increases with the increase of Ma. The wavenumbers of most unstable mode for Fig. 7(a)–(d) are $k_m = 2.36$, 2.44, 2.53, 2.69. In the nonlinear stage, as shown in Fig. 7(a)–(d), the average wavenumber is 1.88, 2.09, 2.51 and 2.51. It seems that at the nonlinear stage, the average wavenumber of the beads are smaller than that predicted by linear stability analysis. The reason is that in the nonlinear stage, the interface consists of several families of quasi-steady travelling waves but separated by different lengths of gaps.

For $a = 0.2$, $Bo = 0.2$, $Bi = 100$, the flow is absolutely unstable for $Ma = 0$ to 1.0 as shown in Fig. 3(b). As shown in Fig. 8, the interface has broken up into a series of beads. In Fig. 8(a) for $Ma = 0$, the film consists of beads with similar structures which is enlarged in Fig. 8(c). In Fig. 8(b) for $Ma = 1.0$, beads with different shapes are distributed in an irregular way. As shown in Fig. 8(b) which is partially enlarged in Fig. 8(d), some beads with large size accompany with smaller droplets.

For $a = 0.2$, $Bo = 0.5$, $Bi = 100$, as shown in Fig. 3(b) the flow is convectively unstable for $Ma = 0$. With the increase of Ma, the flow becomes absolutely unstable. In Fig. 9(a)–(c), no breakup occurs and the interface is in the form of a travelling wave. With the

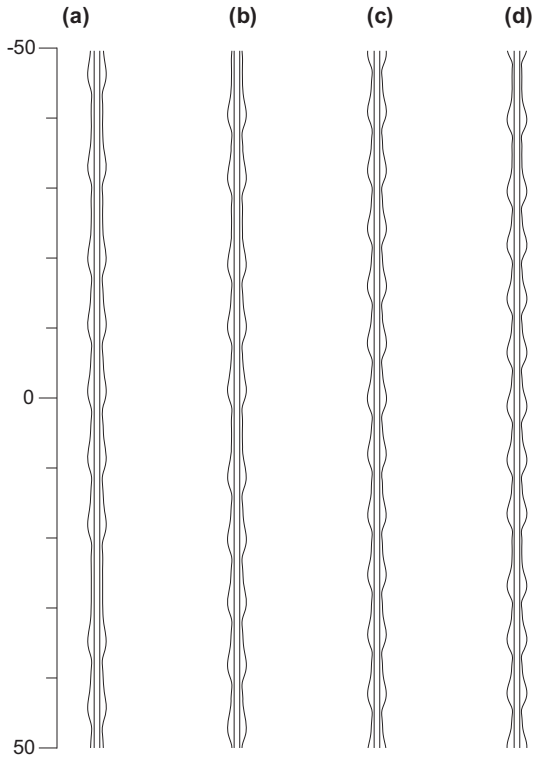

Fig. 7. The profiles of the interface via numerical simulations of Eq. (32) for various Marangoni numbers. Other parameters are $Bo = 0.3$, $Bi = 0.1$, $a = 0.4$. $Ma = 0$, 0.5, 1.0 and 2.0 for (a), (b), (c) and (d). The parameters of (a), (b), (c), (d) are located in the CI regimes. The evolution time of the snapshot is $t = 1000$ for (a), (b), (c), (d).

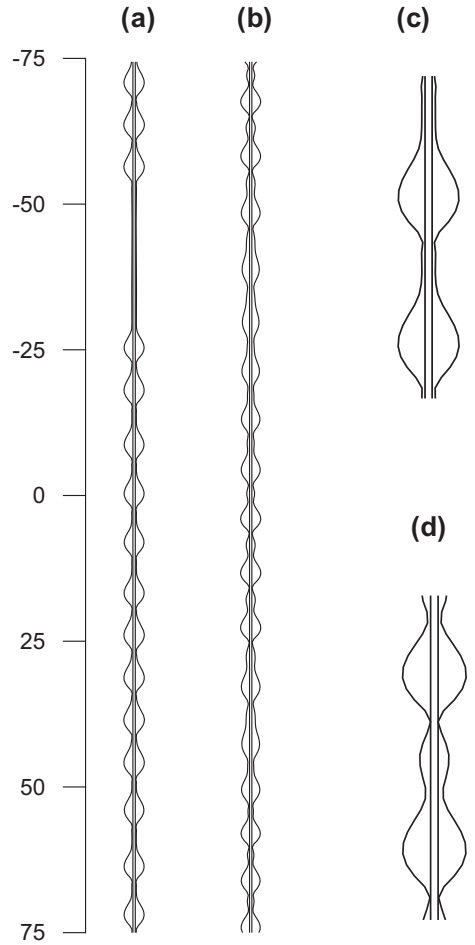

Fig. 8. The profiles of the interface via numerical simulations of Eq. (32) for various Marangoni numbers. Other parameters are $Bo = 0.2$, $Bi = 1.0$, $a = 0.2$. $Ma = 0$, 1.0 for (a), (b). The parameters of (a), (b) are located in the AI regimes. (c) and (d) are the magnifications of the droplets in (a) and (b), respectively. The breakup time $t_b = 23.9$ and 16.1 for (a) and (b).

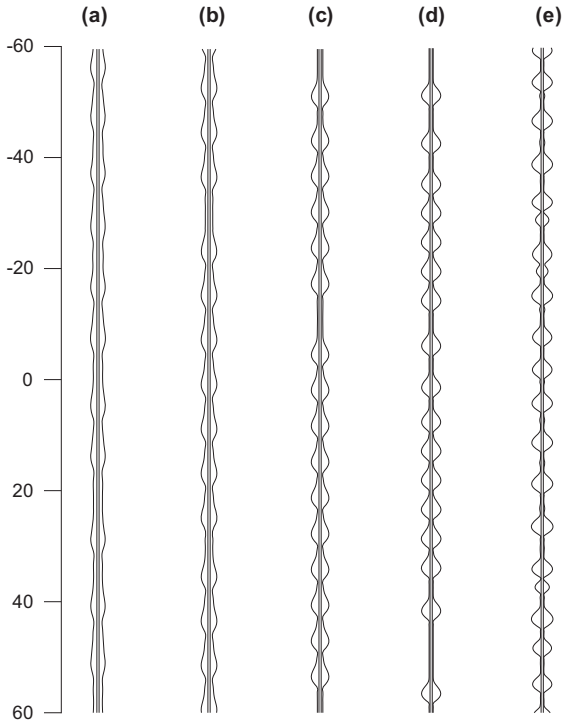

Fig. 9. The profiles of the interface via numerical simulations of Eq. (32) for various Marangoni numbers. Other parameters are $Bo = 0.5,\ Bi = 1.0,\ a = 0.2$. $Ma = 0, 0.5, 1.0, 1.5, 2.0$ for (a), (b), (c), (d), (e). The evolution time of the snapshot is $t = 1000$ for (a), (b), (c). The breakup time $t_b = 28.8$ and 22.1 for (d) and (e).

increase of *Ma*, the beads-like shape becomes more pronounced. As *Ma* increases to 1.5, as shown in Fig. 9(d) the interface breaks up into a series of beads with almost the same size. As *Ma* increases to 2.0, as shown in Fig. 9(e) the interface consists of large beads with almost the same size accompanied with small beads with irregular size.

4. Conclusions

In the present paper, we investigate the dynamics of a coating flow on a fibre driven by the gravity combined with Marangoni effect (thermocapillarity induced by a temperature gradient in the radial direction) in the framework of longwave approximation. A spatio-temporal stability analysis is performed to investigate the convective and absolute instabilities of the film. The results show that the increase of Marangoni effect promotes the absolute instability.

We performed numerical simulations on the nonlinear evolution of axisymmetric disturbances. The breakup behaviour is examined in $a - Bo$ parametric planes for various *Ma* and *Bi*. The result show that most of the breakup points are located in the absolutely unstable regimes, however, at small a it can occur in the convectively unstable regimes. The direct simulations of nonlinear evolution also show that the increase of *Ma* promote the interface to break up into droplets due to the enhancement of the absolute instability. In the no-breakup regimes, the interface is in the form of a travelling wave. With the increase of *Ma*, the beads-like shape of interface becomes pronounced. In the breakup regimes, with the increase of *Ma* the size of beads and the gaps between different beads become more irregular.

Acknowledgments

This work was supported by National Natural Science Foundation of China (Grant Nos. 11102211, 11302236, 11532015).

References

[1] D. Quéré, Fluid coating on a fiber, Annu. Rev. Fluid Mech. 31 (1999) 347–384.
[2] L. Rayleigh, On the instability of a cylinder of viscous liquid under capillary force, Phil. Mag. 34 (1892) 145–154.
[3] D. Quéré, Thin films flowing on vertical fibers, Europhys. Lett. 13 (8) (1990) 347–384.
[4] A.L. Frenkel, "Nonlinear theory of strongly undulating thin films flowing down vertical cylinders, Europhys. Lett. 18 (7) (1992) 583–588.
[5] S. Kalliadasis, H.-C. Chang, Drop formation during coating of vertical fibres, J. Fluid Mech. 261 (1994) 135–168.
[6] H.-C. Chang, E.A. Demekhin, Mechanism for drop formation on a coated vertical fibre, J. Fluid Mech. 380 (1999) 233–255.
[7] I.L. Kliakhandler, S.H. Davis, S.G. Bankoff, Viscous beads on vertical fibre, J. Fluid Mech. 429 (2001) 381–390.
[8] R.V. Craster, O.K. Matar, On viscous beads flowing down a vertical fibre, J. Fluid Mech. 553 (2006) 85–105.
[9] C. Ruyer-Quil, P. Treveleyan, F. Giorgiutti-Dauphiné, C. Dupat, S. Kalliadasis, Modelling film flows down a fibre, J. Fluid Mech. 603 (2008) 431–462.
[10] M. Sweetland, J.H. Lienhard V, Evaporative cooling of continuously drawn glass fibers by water sprays, Int. J. Heat Mass Trans. 43 (5) (2000) 777–790.
[11] L.A. Dávalos-Orozco, X. You, Three-dimensional instability of a liquid layer flowing down a heated vertical cylinder, Phys. Fluids 12 (9) (2000) 1198–2099.
[12] R. Liu, Q.S. Liu, Thermocapillary effect on the dynamics of viscous beads on vertical fiber, Phys. Rev. E 90 (2014) 033005 (1–11).
[13] Z. Ding, T.N. Wong, Three-dimensional dynamics of thin liquid films on vertical cylinders with Marangoni effect, Phys. Fluids 29 (2017) 011701.
[14] M. Moctezuma-Sánchez, L.A. Dávalos-Orozco, Azimuthal instability modes in a viscoelastic liquid layer flowing down a heated cylinder, Int. J. Heat Mass Trans. 90 (2015) 15–25.
[15] R.J. Briggs, Electron-Stream Interaction with Plasmas, MIT, Cambridge, 1964.
[16] A. Bers, Linear waves and instabilities, Physique des Plasmas, in: C. DeWitt, J. Peyraud (Eds.), Gordon & Breach, New York, 1975.
[17] P. Huerre, P.A. Monkewitz, Local and global instabilities in spatially developing flows, Annu. Rev. Fluid Mech. 22 (1990) 473–537.
[18] S.W. Joo, S.H. Davis, Instabilities of three-dimensional viscous falling films, J. Fluid Mech. 242 (1992) 529–547.
[19] C. Duprat, C. Ruyer-Quil, S. Kalliadasis, F. Giorgiutti-Dauphiné, Absolute and convective instabilities of a viscous film flowing down a vertical fiber, Phys. Rev. Lett. 82 (2007) 244502 (1–4).
[20] G. Balestra, M. Gloor, L. Kleiser, Absolute and convective instabilities of heated coaxial jet flow, Phys. Fluids 27 (2015) 054101 (1–17).